AIP | Applied Physics Letters

Ternary eutectic growth of nanostructured thermoelectric Ag-Pb-Te materials

Hsin-jay Wu, Wei-jian Foo, Sinn-wen Chen, and G. Jeffrey Snyder

Citation: Appl. Phys. Lett. **101**, 023107 (2012); doi: 10.1063/1.4733661
View online: http://dx.doi.org/10.1063/1.4733661
View Table of Contents: http://apl.aip.org/resource/1/APPLAB/v101/i2
Published by the American Institute of Physics.

Related Articles

Selective growth of ZnO nanorods and their applications to ferroelectric nanorods
J. Appl. Phys. 112, 034111 (2012)

Biological colloid engineering: Self-assembly of dipolar ferromagnetic chains in a functionalized biogenic ferrofluid
Appl. Phys. Lett. 101, 063701 (2012)

Self-assembly of single dielectric nanoparticle layers and integration in polymer-based solar cells
Appl. Phys. Lett. 101, 063105 (2012)

Patterned substrates to facilitate long-range ordering in the formation of nanoparticle monolayers by electrophoretic deposition
Appl. Phys. Lett. 101, 043117 (2012)

High compositional homogeneity in In-rich InGaAs nanowire arrays on nanoimprinted SiO2/Si (111)
Appl. Phys. Lett. 101, 043116 (2012)

Additional information on Appl. Phys. Lett.

Journal Homepage: http://apl.aip.org/
Journal Information: http://apl.aip.org/about/about_the_journal
Top downloads: http://apl.aip.org/features/most_downloaded
Information for Authors: http://apl.aip.org/authors

ADVERTISEMENT

Downloaded 10 Aug 2012 to 131.215.220.186. Redistribution subject to AIP license or copyright; see http://apl.aip.org/about/rights_and_permissions

Ternary eutectic growth of nanostructured thermoelectric Ag-Pb-Te materials

Hsin-jay Wu,[1] Wei-jian Foo,[2] Sinn-wen Chen,[1,a)] and G. Jeffrey Snyder[3,a)]
[1]*Department of Chemical Engineering, National Tsing Hua University, #101, Sec. 2, Kuang-Fu Rd., Hsin-Chu 300, Taiwan*
[2]*Engineering Science Programme, National University of Singapore, Blk EA, #06-10, 9 Engineering Drive, Singapore 117576*
[3]*Materials Science, California Institute of Technology, 1200 California Blvd., Pasadena, California 91125, USA*

(Received 16 May 2012; accepted 19 June 2012; published online 10 July 2012)

Nanostructured Ag-Pb-Te thermoelectric materials were fabricated by unidirectionally solidifying the ternary Ag-Pb-Te eutectic and near-eutectic alloys using the Bridgeman method. Specially, the Bridgman-grown eutectic alloy exhibited a partially aligned lamellar microstructure, which consisted of Ag_5Te_3 and Te phases, with additional 200-600 nm size particles of PbTe. The self-assembled interfaces altered the thermal and electronic transport properties in the bulk Ag-Pb-Te eutectic alloy. Presumably due to phonon scattering from the nanoscale microstructure, a low thermal conductivity ($\kappa = 0.3$ W/mK) was achieved of the eutectic alloy, leading to a zT peak of 0.41 at 400 K. © *2012 American Institute of Physics*. [http://dx.doi.org/10.1063/1.4733661]

Thermoelectric (TE) materials have long been recognized as a promising candidate in the application of sustainable energy. Nanostructuring in TE material has been considered as an effective way of reducing thermal conductivity while minimizing the decrease of electronic mobility.[1–3] Embedded nanosized phases that created extra interfaces with submicron spacing length are capable of scattering the phonons with mid-to-long mean-free-path.[4] Approaches to synthesize bulk nanostructured materials include solid-state precipitation,[5,6] eutectoid decomposition,[7,8] spinodal decomposition,[9,10] and eutectic reaction,[11,12] etc.

Research on the ternary Ag-Pb-Te system is mostly concentrated on the pseudo-binary PbTe-Ag_2Te owing to the excellent thermoelectric materials PbTe and Ag_2Te.[13,14] Exploration of this ternary system deviated from the pseudo-binary line (PbTe-Ag_2Te) is rare, leaving a large space open for other promising candidates for thermoelectric applications.

This study focuses on the use of ternary eutectics to produce fine microstructures that would be ideal for thermoelectric applications.[11,12] It is proposed by the authors that an Ag-Pb-Te ternary-eutectic ($L \rightarrow Ag_5Te_3 + Te + PbTe$ at 339 °C) featured self-assembled nanostructuring lamellae may be promising for TE applications.[15] Given that the ternary eutectic alloy possesses stronger mechanical strength and promising thermoelectric properties (i.e., composed of a semiconductor PbTe and a metal phase[11]), a synthesis route is carried out, by using the modified Bridgman method,[16,17] with compositions lying close to the Ag-Pb-Te ternary-eutectic point.[17]

The synthesis process started with pure elements; Ag shots (99.99 wt. %, Aldrich, USA), Te flakes (99.99 wt. %, Aldrich, USA), and Pb chunks (99.99 wt. %, Strem chemicals, Newburyport, USA) were weighed based on the compositions listed in Table I and placed in a quartz tubes of 10^{-5} Torr. The total amount of constituent elements was 7.0 g. The ampoules were sealed and homogenized in a furnace at 850 °C for 24 h, followed by water-quenched. The as-prepared ingots were used for unidirectionally solidification, by using the modified Bridgman method.[16,17] The as-solidified plate sample with relative high density (>95%, as listed in Table I) was used for metallographic observations by using a field-emission scanning electron microscope (FE-SEM, Carl Zeiss LEO 1550VP) equipped with a back-scattered electron (BSE) detector. An energy dispersive spectrometer (EDS, Oxford 6587, England) was used for chemical compositional analysis. A powder x-ray diffractometer (Philips X-Pert Pro; Cu Kα radiation) was used for phase identification for angles (2θ) of 20°-90°.

The as-solidified plate sample was polished for thermoelectric property measurements. The thermal conductivity (κ) can be calculated by the equation: $\kappa = C_p D d$, where d is the sample density, C_p is the heat capacity, and D is the thermal diffusivity that determined by using a flash diffusivity method (Netzsch LFA 457). Heat capacity (C_p) is estimated by using Dulong-Petit method, $C_p = 3R/M$. Electrical resistivity (ρ), carrier concentration (n), and carrier mobility (μ) were measured by the Van der Pauw method with a reversible magnetic field of 2.0T. Seebeck coefficient was measured by using chromel-niobium thermocouples of a computer-aided apparatus.[18]

TABLE I. Nominal compositions of the Ag-Pb-Te alloys.

	Composition (at. %)			Density	Relative density	Heat capacity
	Ag	Pb	Te	(g/cm^3)	(%)[a]	(J/gK)
Eutectic	33.1	4.3	62.6	6.60	95.5	0.199
Near-eutectic	31.8	3.1	65.1	6.65	96.2	0.200

[a]The relative density is compared with the theoretical density ($D_{theoretical}$) calculated from each constituent phases, i.e., $D_{theoretical} = 8.4\% \times$ PbTe (8.24 g/cm^3) + $38.3\% \times Ag_5Te_3$ (7.60 g/cm^3) + $53.3\% \times$ Te (6.23 g/cm^3).

a)Authors to whom correspondence should be addressed. Electronic addresses: jsnyder@caltech.edu and swchen@mx.nthu.edu.tw.

 © 2012 American Institute of Physics

Downloaded 10 Aug 2012 to 131.215.220.186. Redistribution subject to AIP license or copyright; see http://apl.aip.org/about/rights_and_permissions

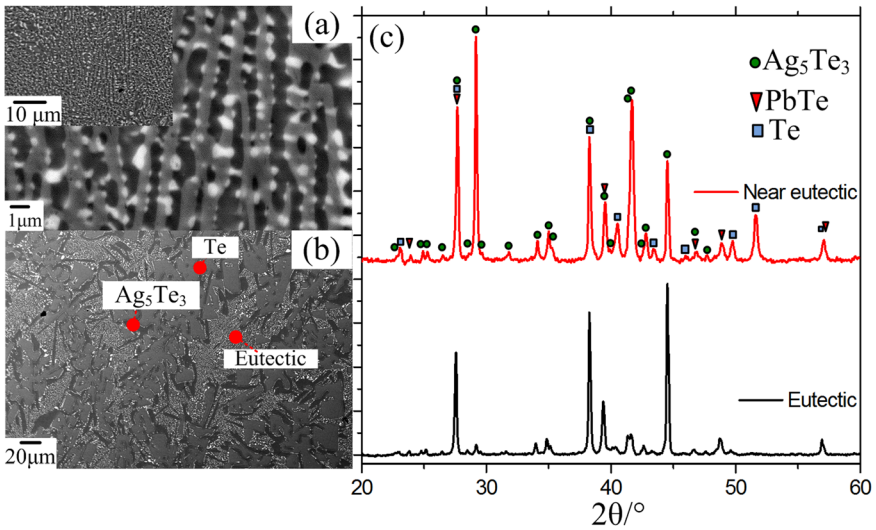

FIG. 1. BEI images of Bridgman-grown (a) eutectic alloy (Ag-4.3 at. %Pb-62.6 at. %Te), (b) near-eutectic alloy (Ag-3.1 at. %Pb-65.1 at. %Te), and (c) XRD patterns of Bridgman-growth eutectic and near-eutectic alloys.

Fig. 1(a) shows the BEI micrograph of the ternary eutectic alloy (Ag-4.3 at. %Pb-62.6 at. %Te) solidified using the Bridgman method; a small picture, shown in the upper-left corner of Fig. 1(a), suggests that no obvious primary phase is found. In Fig. 1(a), the as-solidified eutectic microstructure features a submicron lamellae, composed by the Ag_3Te_5 and the Te phases, and a bright PbTe phase with feature size of 200-600 nm. The overall composition of observed area in Fig. 1(a) is Ag-4.2 at. %Pb-62.6 at. %Te, close to the starting composition of the eutectic alloy, Ag-4.3 at. %Pb-62.6 at. %Te.

Similarly, a near-eutectic alloy with composition of Ag-3.1 at. %Pb-65.1 at. %Te is also solidified using the Bridgman method (Fig. 1(b)), revealing a distinct microstructure. As shown in Fig. 1(b), the primary phase is recognized as the Te phase, the secondary phase is Ag_5Te_3 with composition of Ag-37.8 at. %Te, and the fine region, which is the last solidification region, is the ternary eutectic with average composition of Ag-4.3 at. %Pb-63.2 at. %Te. Fig. 1(c) shows the x-ray diffraction patters of the eutectic and near-eutectic alloys. Three different phases can be identified, Ag_5Te_3 (JCPDS#861168), PbTe(JCPDS#381435), and Te(JCPDS#361452).

The performance of thermoelectric material is guided by the figure-of-merit (zT), $zT = (S^2/\rho\kappa)T$, where S is the Seebeck coefficient, ρ is the electrical resistivity, κ is the thermal conductivity, and T is the absolute temperature, respectively. Fig. 2(a) shows the thermal conductivity (κ) of those two alloys. Generally, the thermal conductivity (κ) contains two contributions ($\kappa = \kappa_L + \kappa_e$); the lattice thermal conductivity (κ_L) and electronic thermal conductivity (κ_e). The κ_e is further expressed by the Wiedemann-Franz law: $\kappa_e = LT/\rho$, where L is the Lorenz factor ($L = 2.45 \times 10^{-8}\ V^2/K^2$, for free electrons). However, in our case, the electronic terms (κ_e) are less than 5% of the overall thermal conductivity (i.e., $\kappa_e < 0.02$ W/mK). Thus, the lattice term dominates the thermal conductivity, and the electrical term can be neglected. The eutectic alloy exhibits lower thermal conductivity than that of the near-eutectic; a minimum value of 0.3 W/mK at 415 K is found in the eutectic alloy.

Fig. 2(b) shows the Seebeck coefficients and electrical resistivity of the eutectic and near-eutectic alloys. The Seebeck coefficients are all positive in the temperature range of 300-430 K, revealing p-type behavior. At 300 K, the Seebeck coefficient of the near-eutectic alloys is larger than 420 (μV/K), while that of the eutectic alloy is relatively smaller ($S = 395\ \mu$V/K). On the other hand, it is suggested from Fig. 2(b) that the near-eutectic alloy, which has a higher Seebeck coefficient, exhibits higher electrical resistivity (denoting as open circles) and gradually decreases with

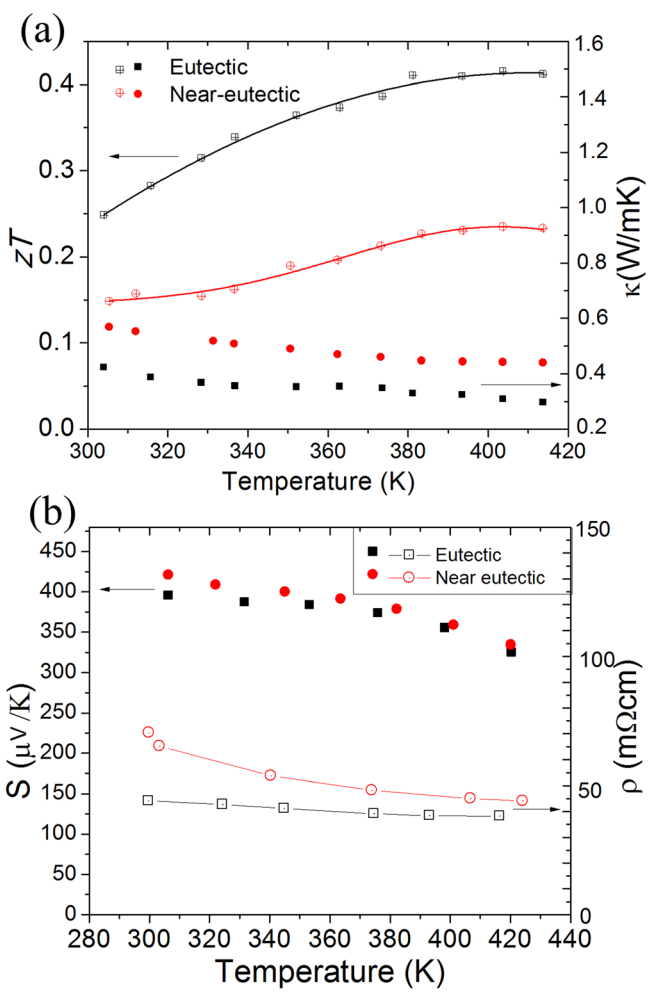

FIG. 2. Temperature-dependent (a) thermal conductivity and figure-of-merit (zT) and (b) Seebeck coefficients and electrical resistivity of eutectic and near-eutectic alloys.

Downloaded 10 Aug 2012 to 131.215.220.186. Redistribution subject to AIP license or copyright; see http://apl.aip.org/about/rights_and_permissions

temperatures. The electrical resistivity of the eutectic alloy (denoting as open squares) is almost temperature-independent. It is possible that the nanostructure of the eutectic alloy with interface spacing less than 1 μm is attributed to enhance the scattering of phonons with long mean-free-path and thus reduces the thermal conductivity (Fig. 2(a)). Furthermore, the partially aligned lamellae (i.e., $Ag_5Te_3 + Te$) is likely to provide a continuous electronic transport path that gives a lower electrical resistivity.[4] Nanorods of Te are known to be semiconducting with good thermoelectric properties.[19]

In general, a promising thermoelectric material should possess large Seebeck coefficient, which corresponds to low carrier concentration, and large electrical conductivity ($\delta = 1/\rho$), which requires high carrier concentration. Thus, an optimal carrier concentration, which is typically found in heavily doped semiconductors ($n \sim 10^{19}$-10^{21} carrier/cm^3, Ref. 20), is crucial to obtain a balance between the Seebeck coefficient and electrical conductivity. The dependences of the Seebeck coefficient (assuming a degenerate semiconductor or metal with acoustic phonon scattering) and the electrical conductivity with carrier concentration n can be expressed as Eqs. (1) and (2), respectively.

$$S = \frac{8\pi^2 k_B^2}{3eh^2} m^* T \left(\frac{\pi}{3n}\right)^{2/3}, \quad (1)$$

$$\frac{1}{\rho} = \sigma = ne\mu, \quad (2)$$

where m^* is the effective mass and μ is the carrier mobility, respectively. It is expected that the Seebeck coefficients and the electrical resistivity decreases as the carrier concentration increases ($S \sim n^{-2/3}$ and $\rho \sim n^{-1}$), respectively.

The experimental Hall carrier concentration (n_H) is calculated via $n_H = 1/eR_H$, where e is the electron charge and R_H is Hall coefficient. The temperature dependent Hall carrier concentration (n_H) of the eutectic and near-eutectic alloys is shown in Fig. 3(a). If the conduction is dominated by a single band and the scattering is known, the relationship between the actual carrier concentration (n) and the measured Hall carrier concentration (n_H) can be calculated.[21] However, the Seebeck and resistivity of the alloys reported here decrease with temperature which suggests multiple, not single band behavior. Furthermore, because of the complex composite microstructure the analysis of Hall coefficient derived for homogeneous materials should not be considered quantitatively precise.

Nevertheless, the analysis of the experimental Hall coefficient (R_H) using the more familiar quantities of Hall carrier concentration (n_H) and Hall mobility ($\mu_H = R_H/\rho$) can lead to insight and qualitative comparisons. As shown in Fig. 3(a), the Hall carrier concentration of those two alloys are roughly in the same order of magnitude, $10^{17} \sim 10^{18}$ (carrier/cm^3). The eutectic alloy has slightly higher Hall carrier concentration compared with that of the near-eutectic alloy, which may explain the lower Seebeck coefficient as shown in Fig. 2(b).

Hall carrier mobility, μ_H, of the eutectic and near-eutectic alloys (Fig. 3(b)), shows similar values. The

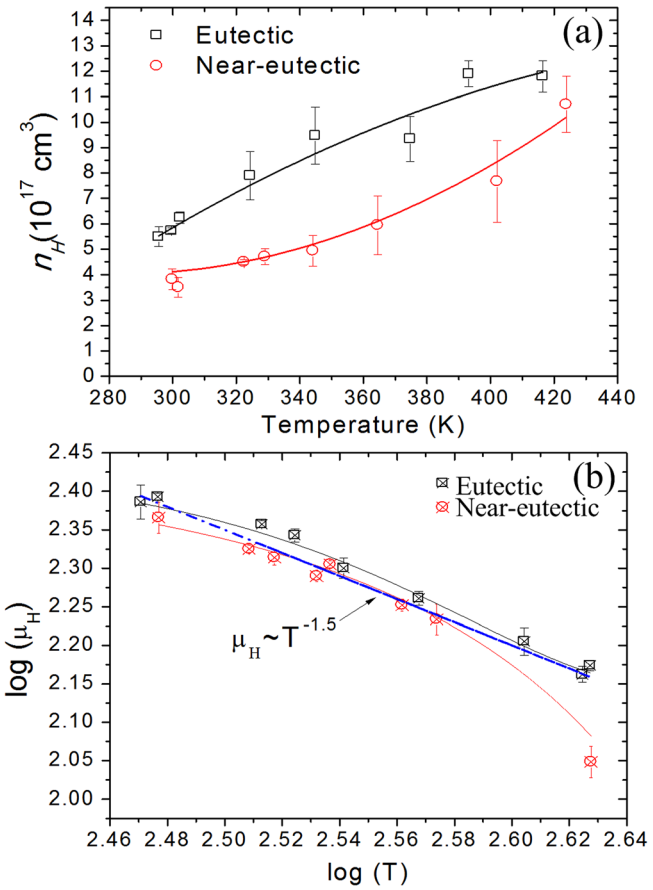

FIG. 3. Temperature-dependent (a) Hall carrier concentration (n_H) and (b) Hall carrier mobility (μ_H) of eutectic and near-eutectic alloys.

decrease in Hall mobility with temperature follows a power law approximately as $\mu \sim T^{-1.5}$ (denoting by a dashed line), suggesting that acoustic scattering dominates in both eutectic and near-eutectic alloys.[21,22]

The temperature dependent figure-of-merit (zT) is shown in Fig. 2(a). The zT of the eutectic alloy gradually increase with temperature and reach its maximum value of 0.41 at 400 K. The zT values of the near-eutectic are lower than that of the eutectic one, with a maximum zT peak of 0.23 at 400 K.

In summary, an approach for synthesis of aligned nanostructured bulk thermoelectric material, using unidirectional solidification, is demonstrated with ternary eutectic and near-eutectic Ag-Pb-Te alloys. The ternary Ag-Pb-Te eutectic featured nanosized lamellar structure which consisted of Ag_5Te_3 and Te, and nanoinclusions of PbTe phase. The ternary eutectic Ag-Pb-Te alloy exhibits low thermal conductivity (0.3 W/mK at 415 K), presumably due to the nanosized lamellar structure and the nanoinclusions that enhance phonon scattering. Furthermore, the partially aligned lamella ($Ag_5Te_3 + Te$) could be beneficial to the electrical transport, yielding a ZT maximum of 0.41 at 400 K. Given that the Hall carrier concentrations of the alloys (10^{17}-10^{18} carrier/cm^3) are still lower than that of optimal range (10^{19}-10^{21} carrier/cm^3), further engineering of the carrier concentration may further improve the thermoelectric performance.

The authors acknowledge the financial support of National Science Council of Taiwan (NSC 99-2221-E-007-093-MY3 and Grant 100-2917-I-007-001) and of the Air

Downloaded 10 Aug 2012 to 131.215.220.186. Redistribution subject to AIP license or copyright; see http://apl.aip.org/about/rights_and_permissions

Force Office of Scientific Research (AFOSR MURI FA9550-10-1-0533) of USA.

[1]Y. Pei, J. Lensch-Falk, E. S. Toberer, D. L. Medlin, and G. J. Snyder, Adv. Funct. Mater. **21**, 241 (2010).
[2]G. J. Snyder and E. S. Toberer, Nat. Mater. **7**, 106 (2008).
[3]M. G. Kanatzidis, Chem. Mater. **22**, 648 (2010).
[4]D. L. Medlin and G. J. Snyder, Curr. Opin. Colloid. Interface Sci. **14**, 226 (2009).
[5]T. Ikeda, N. J. Marolf, and G. J. Snyder, Cryst. Growth Des. **11**, 4183 (2011).
[6]T. Ikeda, M. B. Toussaint, K. Bergum, S. Iwanaga, and G. J. Snyder, J. Mater. Sci. **46**, 3846 (2011).
[7]T. Ikeda, E. S. Toberer, R. V. Ravi, G. J. Snyder, S. Aoyagi, E. Nishiboric, and M. Sakata, Scr. Mater. **60**, 321 (2009).
[8]T. Ikeda, L. A. Collins, V. A. Ravi, F. S. Gascoin, S. M. Haile, and G. J. Snyder, Chem. Mater. **19**(4), 763 (2007).
[9]J. He, S. N. Girard, M. G. Kanatzidis, and V. P. Dravid, Adv. Funct. Mater. **20**, 764 (2010).
[10]S. Gorsse, P. Bellanger, Y. Brechet, E. Sellier, A. Umarji, U. Ail, R. Decourt, Acta Mater. **59**, 7425 (2011).
[11]J. R. Sootsman, J. He, V. P. Dravid, C. P. Li, C. Uher, and M. G. Kanatzidis, J. Appl. Phys. **105**, 083718 (2009).
[12]H. J. Wu and S. W. Chen, J. Alloys Compd. **509**, 656 (2011).
[13]K. Bergum, T. Ikeda, and G. J. Snyder, J. Solid State Chem. **184**, 2543 (2011).
[14]J. L. Lensch-Falk, J. D. Sugar, M. A. Hekmaty, and D. L. Medlin, J. Alloys Compd. **504**, 37 (2010).
[15]H. J. Wu, W. J. Foo, W. Gierlotka, G. J. Snyder, and S. W. Chen, "Microstructures, liquidus projection and thermodynamic modeling of thermoelectric Ag-Pb-Te system," (unpublished).
[16]H.-J. Wu, S.-W. Chen, T. Ikeda, and G. J. Snyder, Acta Mater. **60**, 1129–1138 (2012).
[17]H.-J. Wu, S.-W. Chen, T. Ikeda, and G. J. Snyder, "Reduced thermal conductivity in Pb-alloyed $AgSbTe_2$ thermoelectric materials," (unpublished).
[18]S. Iwanaga, E. S. Toberer, A. LaLonde, and G. J. Snyder, Rev. Sci. Instrum. **82**, 063905 (2011).
[19]K. C. See, J. P. Feser, C. E. Chen, A. Majumdar, J. J. Urban, and R. A. Segalman, Nano Lett. **10**(11), 4664 (2010).
[20]E. S. Toberer, A. F. May, and G. J. Snyder, Chem. Mater. **22**, 624 (2010).
[21]A. F. May, E. S. Toberer, A. Saramat, and G. J. Snyder, Phys. Rev. B **80**, 125205 (2009).
[22]R. A. Smith, *Semiconductors*, 2nd ed. (Cambridge University Press, Cambridge, 1978).

Downloaded 10 Aug 2012 to 131.215.220.186. Redistribution subject to AIP license or copyright; see http://apl.aip.org/about/rights_and_permissions